Compensation of distant phase-distorting layers. II. Extended-field-of-view adaptive receiver system

Mikhail A. Vorontsov

Intelligent Optics Laboratory, Computational and Information Sciences Directorate, U.S. Army Research Laboratory, Adelphi, Maryland 20783, and Intelligent Optics Laboratory, Institute for Systems Research, University of Maryland, College Park, Maryland 20742

Miao Yu

Intelligent Optics Laboratory, Institute for Systems Research, University of Maryland, College Park, Maryland 20742

We analyze the anisoplanatic adaptive receiver system field of view (FOV) and the possibility of controlling the system FOV by using an adaptive optics system with multiple wave-front sensors that sense wave-front phase aberrations of reference waves with different arrival angles. The conventional decoupled stochastic parallel gradient descent (D-SPGD) technique is generalized to include output signals from multiple wave-front sensors. The multiple-reference D-SPGD control algorithm introduced here is applied to obtain an anisotropic FOV in adaptive receiver systems by using two and three reference waves. © 2004 Optical Society of America

OCIS codes: 010.1080; 010.0010; 110.0110.

1. INTRODUCTION

In Part I of this paper (see Ref. 1) adaptive receiver systems based on stochastic parallel gradient descent (SPGD),[2,3] decoupled stochastic parallel gradient descent (D-SPGD),[4] and phase-conjugation (PC)[5] algorithms were analyzed for the case in which propagation medium inhomogeneities cannot be approximated by a single phase-distorting layer located at the receiver system pupil plane (pupil-plane phase screen). The propagation medium models included a single remote phase-distorting layer and a set of phase-distorting layers equidistantly distributed along the propagation path.

In these propagation scenarios, the effect of the distant distorting layer(s) emerges in the receiver telescope pupil plane as nonuniform intensity distributions (known as scintillations) and as complicated wave-front phase-aberration patterns that can contain phase singularities (branch points and 2π phase cuts). Both effects—scintillations and phase singularities—are highly undesirable and can result in degradation of compensation performance, as discussed in Part I.

The distant location of phase inhomogeneities (distant phase-distorting layers) results in another important effect known as angular anisoplanatism.[6,7] The optical waves emerging at the receiver telescope undergo phase aberrations dependent on their arrival angle. In the adaptive systems considered in Part I, phase-aberration compensation is based solely on the sensing of on-axis wave aberrations (on-axis compensation). The efficiency of this on-axis compensation degrades with the increase of the wave arrival angle, resulting in narrowing the

adaptive optics receiver system field of view (FOV) imposed by angular anisoplanatism.[6–8]

Analysis of the effect of the remotely located phase-distorting layers on the adaptive optics receiver system FOV, as well as the possibilities for extending the receiver system FOV (extended-field-of-view compensation), are important issues for many adaptive optics applications.[9–12] Here in Part II we address these problems by considering adaptive (closed-loop) compensation of distant phase-distorting layers with use of the D-SPGD and SPGD adaptive optics control system architectures.

In Section 2, efficiency of narrow-FOV (on-axis) D-SPGD compensation is analyzed for wave components that enter a remotely located phase-distorting layer at different offset angles (off-axis waves), propagate to the receiver telescope, and undergo only on-axis phase compensation. In Section 3, we discuss a new closed-loop correction algorithm designed to operate with multiple reference waves originating from multiple-reference light sources or guide stars. This algorithm—multireference (MR) D-SPGD—provides adaptive correction over a wider FOV (extended-FOV compensation) than does on-axis compensation with a single reference wave. The MR D-SPGD controller does not require knowledge of either the strength or the position of distorting layers and can operate with a single or multiple wave-front correctors.

Examples of MR D-SPGD compensation are described in Section 4. They include extended-FOV compensation inside a one-dimensional angular region and extended-FOV correction inside a finite two-dimensional angular region. Extended-FOV compensation is performed by using an adaptive system with a MR D-SPGD controller, a

single wave-front corrector, and multiple (two or more) narrow-FOV wave-front sensors capable of independently sensing phase aberrations originating from different reference waves.

2. ADAPTIVE RECEIVER FIELD-OF-VIEW FOR ON-AXIS COMPENSATION

A. Adaptive Optics Receiver System with On-Axis Compensation: Numerical Models

Consider an adaptive receiver system operating with a single phase-distorting layer located a distance l from the telescope pupil, as shown in Fig. 1. The feedback control system is composed of a beam splitter, BS, a wave-front sensor, WFS, a lens L_s that re-images the telescope pupil plane to the wave-front sensor input plane, a D-SPGD controller, and a wave-front corrector with an aperture size of D_c (controllable mirror array of $N = n_c \times n_c$ piston-type actuators). The wave-front sensor (the point-diffraction interferometer described in Part I) provides sensing of phase aberrations only for the on-axis reference wave (narrow-FOV wave-front sensor). This can be achieved by filtering the off-axis wave components in the receiver telescope (lens L) focal plane using a small diaphragm, D. Compensation efficiency of the D-SPGD adaptive optics system in Fig. 1 was analyzed in Part I for on-axis waves (narrow-FOV compensation).

Consider now an off-axis wave that propagates in the direction of the angular vector $\boldsymbol{\theta} = \{\theta_x, \theta_y\}$, where θ_x and θ_y are angular coordinates. To simplify the analysis assume that $\theta_x = \theta$, $\theta_y = 0$, and $\theta \ll 1$ (small-angle approximation).

The distant phase-distorting layer introduces the phase perturbation $\varphi(\mathbf{r})$ into both on- and off-axis waves. From the wave propagation geometry in Fig. 1, it follows that the off- and on-axis waves are mutually shifted by a distance $\Delta \cong l\theta$ at the phase-distorting layer plane ($z = 0$). This linear shift leads to a corresponding shift between the pupil-plane phase-aberration functions for the on-axis $\varphi_p(\mathbf{r})$ and the off-axis $\varphi_p^\theta(\mathbf{r})$ waves: $\varphi_p^\theta(x, y) = \varphi_p(x + \Delta, y)$. Here we neglect the difference in the length of the propagation path by assuming that $\Delta \ll l$.

The adaptive phase correction $u(\mathbf{r})$ is obtained by sensing the phase aberrations only of the on-axis reference wave. As a result, compensation efficiency (measured by the Strehl ratio St or some other metric) depends on the wave arrival angle θ (viewing direction).[7] The dependence of the Strehl ratio $St(\theta)$ on the viewing direction characterizes the compensated receiver system FOV.

Typically in the analysis of anisoplanatic effects, wave propagation between the phase-distorting layer and the receiver system aperture is described by using the geometrical optics approximation, so that pupil-plane intensity scintillations, as well as the difference between the pupil-plane phase $\varphi_p(\mathbf{r})$ and the induced phase perturbation $\varphi(\mathbf{r})$, are ignored.[11,12] This approach is often referred to as the near-field approximation or the phase-aberration projection approximation.[7] In this approximation $\varphi_p(\mathbf{r}) \cong \varphi(\mathbf{r})$ and hence $\varphi_p^\theta(x, y) = \varphi_p(x + \Delta, y)$.

We also analyze a more general approach in which the propagation of both the off- and the on-axis waves are described by using the parabolic approximation of the wave propagation equation, often known as the quasi-optical approximation [see Eq. (6) in Part I]. This approximation accounts for diffraction effects and hence for both intensity scintillations and phase singularities.

In the numerical analysis of the adaptive optics system in Fig. 1 the complex amplitude of the off-axis wave arriving at the telescope pupil at the angle θ is obtained by considering propagation of the on-axis wave that passes through the distorting layer shifted by the distance $\Delta = l\theta$.

For the offset angle θ, the phase perturbation introduced by the shifted distorting layer is $\varphi^\theta(x, y) = \varphi(x + \Delta, y)$ or, equivalently, $\varphi^\theta(x, y) = \varphi(x + l\theta, y)$. The phase control $u(\mathbf{r})$ is assumed to be the same for all of the offset angles θ inside the angular region Ω_θ. The residual phase aberration $\delta^\theta(\mathbf{r}) = \varphi^\theta(\mathbf{r}) + u(\mathbf{r})$, as well as the Strehl ratio $St(\theta)$, are functions of the offset angle θ. The Strehl ratio $St(\theta)$ is defined as the ratio of the on-axis focal-plane intensity for the corrected wave (obtained by using the distorting layer shifted by $\Delta = l\theta$) to the corresponding on-axis focal-plane intensity in the absence of aberrations. The phase correction function $u(\mathbf{r})$ is obtained by using the D-SPGD control algorithm applied only to the on-axis reference wave, as described in Part I [see Eq. (2) there].

Similar to the numerical analysis in Part I, the phase perturbations $\varphi(\mathbf{r})$ introduced here correspond to realizations of the random function with zero mean and the Andrews model of the atmospheric turbulence power spectrum [Eq. (10) in Part I]. Phase-perturbation strength is characterized by the ratio D_c/r_0, where r_0 is the Fried parameter.

In the numerical simulations, the complex amplitude of the waves entering the phase-distorting layer corresponds to a super-Gaussian beam with radius $a = 1.5 D_c$, as described by Eq. (8) in Part I.

It is convenient to normalize the offset angle by the parameter $\theta_D = D_c/l$ so that the normalized offset angle is given by $\tilde{\theta} = \theta/\theta_D$. The parameter θ_D is the viewing angle at which the receiver aperture of size D_c is seen from an on-axis point at the distorting layer plane. Note that from the relationship $\Delta = \theta l$ it follows that $\tilde{\theta} = \tilde{\Delta}$, where $\tilde{\Delta} = \Delta/D_c$.

Computation of the on-axis compensation control function $u(\mathbf{r})$ and the corresponding angular dependence $St(\tilde{\theta})$ was repeated for 50 realizations of the phase-
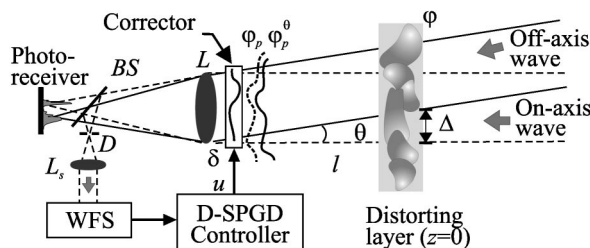

Fig. 1. Schematic of adaptive system with D-SPGD controller and a single distant phase-distorting layer located at the plane $z = 0$.
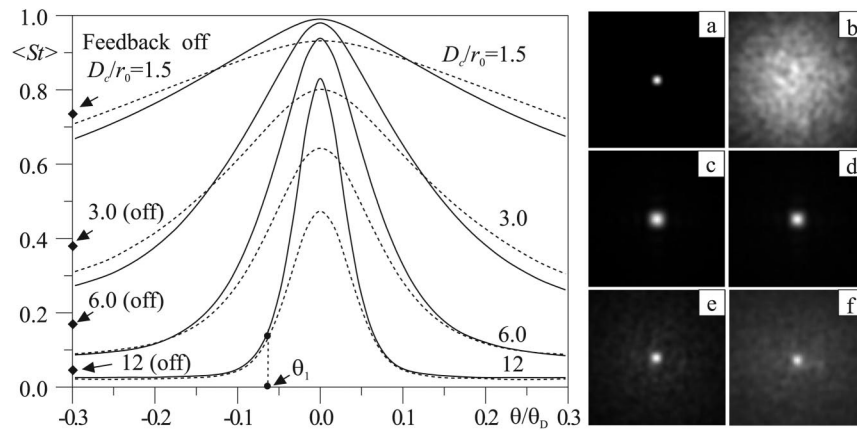
Fig. 2.   Angular dependence of the ensemble-averaged Strehl ratio $\langle St \rangle$ for D-SPGD adaptive on-axis compensation of a distant phase-distorting layer for different values of D_c/r_0:   near-field approximation (solid curves) and quasi-optical approximation (dashed curves). The uncompensated Strehl ratio values $\langle St_0 \rangle$ are shown by diamonds.   The gray-scale images at right represent focal-plane intensity distributions: a, diffraction limited and b–f for a phase-distorting layer with $D_c/r_0 = 6$.   Focal-plane intensity distributions are shown, b, for uncompensated and c, d, for compensated on-axis waves, where b and c are obtained in the near field and d in the quasi-optical approximation for $l = 0.03 l_d$ ($l_d = 0.5 k a^2$).   Images e and f are obtained for $\theta = \theta_1 = 0.06 \theta_D$ for the near-field and the quasi-optical approximations ($l = 0.03 l_d$), respectively.   Each intensity distribution in a–f is normalized by its own maximum value.

perturbation random functions $\varphi(\mathbf{r})$.   The obtained Strehl ratio values are ensemble averaged.

B.   Field of View for On-Axis Compensation

Consider numerical analysis results of on-axis compensation with the D-SPGD controller.   Dependence of the ensemble-averaged Strehl ratio $\langle St(\tilde{\theta}) \rangle$ on the normalized offset angle $\tilde{\theta} = \theta/\theta_D$ is shown in Fig. 2 for different D_c/r_0 ratios.   In this figure the solid curves correspond to the near-field approximation [$\varphi_p(\mathbf{r}) = \varphi(\mathbf{r})$], and the dashed curves are obtained by considering wave propagation (diffraction) from the distant phase-distorting layer to the telescope pupil plane using the quasi-optical (parabolic) approximation.

Define the adaptive receiver system FOV as the angular region $\Omega_{\text{FOV}} = \{0 \leq \theta \leq \theta_0\}$ inside which phase compensation results in an averaged Strehl ratio that is increased beyond the uncompensated value $\langle St_0 \rangle$.   The region Ω_{FOV} is commonly referred to as the isoplanatic region, where θ_0 is the isoplanatic angle.   For a single thin layer of Kolmogorov turbulence, $\theta_0 = 0.31(r_0/l)$.[5]

In Fig. 2 the uncompensated values $\langle St_0 \rangle$ are indicated by the diamond symbols on the y axis.   When compared with the uncompensated receiver system, on-axis compensation results in improvement of the Strehl ratio within the isoplanatic region, with the angular size θ_0 decreasing as the turbulence strength increases (increase of the D_c/r_0 ratio).

Compensated focal-plane intensity distributions corresponding to different offset angles are shown in Figs. 2a–2f.   Note that even partial compensation corresponding to relatively large offset angles and small Strehl ratio values [$\langle St(\theta) \rangle \cong 0.1 - 0.2$] can produce a useful result such as the formation of the well-known core-halo images of a point reference source.[13]   As seen in Figs. 2e and 2f, partial compensation obtained for the offset angle $\theta_1 = 0.06\theta_D$ corresponding to $\langle St(\theta_1) \rangle \cong 0.15$ results in a nearly diffraction-limited size of the core in the focal-plane intensity distributions.

Compare the efficiency of on-axis compensation obtained from the quasi-optical (dashed curves in Fig. 2) and the near-field approximations (solid curves in Fig. 2).   As expected from the analysis described in Part I, diffraction effects cause an overall decrease in compensation efficiency for the on-axis waves (decrease in Strehl ratio value for $\theta = 0$).

On the other hand, accounting for diffraction can increase the receiver system FOV (compare solid and dashed curves corresponding to $D_c/r_0 = 1.5$ and $D_c/r_0 = 3$ in Fig. 2).   This increase in the angular compensation range is associated with diffraction-induced filtering of the small-scale phase-aberration components.   When the amplitude of the phase perturbations (turbulence strength) is relatively small, this filtering results in phase smoothing and an increase in the overall correlation distance between the pupil-plane on- and off-axis phase distortions.

As mentioned in Part I, when phase perturbation strength increases, evolution of the phase along the propagation path leads to the appearance of wave-front branch points.   A linear shift in branch-point position occurring for the off-axis waves may strongly affect correlation properties of the wave-front phase for on- and off-axis waves.   This is the reason that the diffraction-induced increase in the receiver system FOV occurs only for relatively weak phase aberrations or short propagation distances.

3.   COMPENSATION WITH MULTIPLE REFERENCES: MULTIREFERENCE DECOUPLED STOCHASTIC PARALLEL GRADIENT DESCENT CONTROLLER

A.   Decoupled Stochastic Parallel Gradient Descent Adaptive Optics System with Multiple References

Consider closed-loop compensation with the use of several reference light sources.   In astronomical and directed energy adaptive optics applications, these reference light

sources are often referred to as guide stars (natural or laser guide-stars).[7,13-18] In free-space laser communication applications, the reference waves (beams) can originate from a set (array) of spatially separated laser transmitters used for mitigation of the atmospheric-turbulence-induced communication signal fading. Using multiple reference waves can extend the receiver system FOV beyond that obtained with on-axis compensation.[10,18,19]

For simplicity, assume that the adaptive receiver system has a single pupil-plane wave-front corrector and operates with only the two reference sources A and B as shown in Fig. 3a. Sampling of the reference waves is performed in parallel with the use of two narrow-FOV wave-front sensors. The small pinholes D_A and D_B located in the receiver system image plane provide narrow-FOV angular filtering of the received waves, so that each wave-
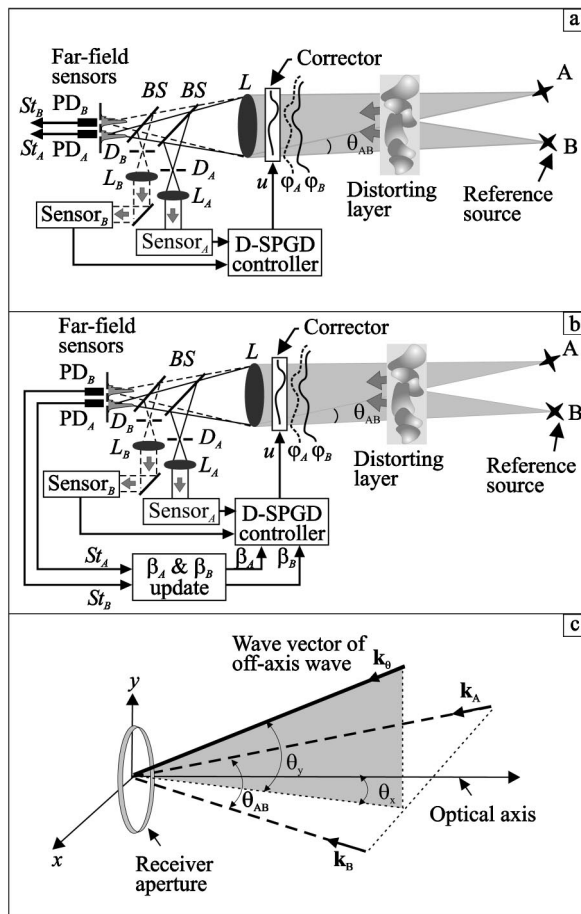

Fig. 3. Schematics of the D-SPGD adaptive receiver systems operating with two reference sources (A and B) and a single wave-front corrector. The two near-field wave-front sensors Sensor$_A$ and Sensor$_B$ are in planes conjugate to the telescope pupil plane formed by beam splitters BS and the re-imaging lenses L_A and L_B. Diaphragms D_A and D_B provide narrow FOV sensing of wave-front distortions corresponding to each of the two reference waves. Feedback control in a is based solely on information obtained from the near-field sensors (conventional D-SPGD controller). The multiple-reference (MR) D-SPGD controller in (b) is based on both far-field (St_A and St_B) and near-field sensor outputs. The far-field sensors are composed of pinhole diaphragms and photodetectors PD$_A$ and PD$_B$. The wave vector geometry for the reference and off-axis waves is illustrated in c.

front sensor can independently sense only the reference field residual phase aberrations (phase errors) $\delta_A(\mathbf{r}) = u(\mathbf{r}) + \varphi_A(\mathbf{r})$ and $\delta_B(\mathbf{r}) = u(\mathbf{r}) + \varphi_B(\mathbf{r})$, where $\varphi_A(\mathbf{r})$ and $\varphi_B(\mathbf{r})$ are the pupil-plane phase aberrations for each of the two reference waves.

B. Performance Metrics for Multiple-Reference Operation

Wave-front control in the adaptive optics receiver system with two references aims to simultaneously decreasing both phase errors, $\delta_A(\mathbf{r})$ and $\delta_B(\mathbf{r})$. This control goal can be achieved by minimizing the following performance metric (phase-error metric):

$$J_\delta[u] \equiv \frac{1}{S} \int_{\Omega_C} [\,\delta_A^2(\mathbf{r}) + \delta_B^2(\mathbf{r})]\mathrm{d}^2\mathbf{r}, \qquad (1)$$

where Ω_C is the wave-front sensor/corrector aperture with an area of S.

The phase-error metric (1) can be minimized in a closed-loop control system based on model-free optimization techniques (gradient-descent,[5] multidithering,[20] SPGD,[2-4] stochastic approximation[21]). Nevertheless, practical implementation of model-free optimization for multiple-reference compensation faces at least two potential problems. First, computation of metric (1) requires phase reconstruction from the wave-front sensor intensity data—essentially the same problem as for closed-loop operation with a single reference. An additional obstacle is that phase reconstruction should be performed in parallel for two sensors. The second problem is associated with the potential risk that the model-free optimization process may converge to only one of the local minima for performance metric (1). The most likely minimum of metric (1) corresponds to compensation of single residual phase errors only: $\delta_A(\mathbf{r})$ or $\delta_B(\mathbf{r})$.

The first problem, the phase reconstruction requirement, can be overcome by using optimization of performance metrics based not on phase but on the output intensity of the near- or far-field wave-front sensors. As an example, consider far-field sensors that provide measurements of the Strehl ratios St_A and St_B associated with each of the reference sources. The performance metric for the adaptive optics system with two references is given by the expression

$$St_{AB} \equiv St_A + St_B. \qquad (2)$$

The metric components St_A and St_B are proportional to the light power inside the small diaphragms (pinholes) D_A and D_B in Fig. 3a. The adaptation goal is to maximize metric (2).

Another performance metric that can be used for multiple-reference operation is similar to the wave-front sensor fidelity metric J_3 discussed in Part I. For the case of two reference waves this metric can be computed by using the intensity distributions $I_\delta^A(\mathbf{r})$ and $I_\delta^B(\mathbf{r})$ obtained from the near-field wave-front sensors:

$$J_3^{AB} = J_3^A + J_3^B = \sum_{j=1}^{N} (\bar{I}_j^A + \bar{I}_j^B)$$

$$= \int_{\Omega_C} I_\delta^A(\mathbf{r})\mathrm{d}^2\mathbf{r} + \int_{\Omega_C} I_\delta^B(\mathbf{r})\mathrm{d}^2\mathbf{r}. \quad (3)$$

The sensor output signals $\{\bar{I}_j^A\}$ and $\{\bar{I}_j^B\}$ in Eq. (3) are proportional to the output intensities $I_\delta^A(\mathbf{r})$ and $I_\delta^B(\mathbf{r})$ integrated over the sensor's subaperture areas $\{\Omega_j\}$ as described in Part I.

Closed-loop optimization of either the far-field metric (2) or the near-field metric (3) does not require wave-front reconstruction. However, the problem of local extrema associated with maximization of the individual metric components St_A or St_B in Eq. (2) or the minimization of the metric components J_3^A or J_3^B in Eq. (3) remains unresolved with conventional optimization techniques.

C. Metric Local Extrema and "Winner-Takes-All" Competition

Generalization of performance metrics (2) and (3) for operation with N_g reference waves (guide stars) can be represented in the form

$$J = \sum_{j=1}^{N_g} \beta_j j_j, \quad (4)$$

where $\{\beta_j\}$ are weighting coefficients and $\{j_j\}$ ($j = 1,...,N_g$) are the metric components corresponding to each of the N_g reference sources.

Adaptive system operation using optimization of the multiple-reference performance metric (4) has essentially the same problem as optimization of metrics (2) or (3): the risk that the adaptation process will be trapped in one of the metric (4) local extrema typically associated with each reference wave. As the number of references N_g increases, the problem of local extrema becomes more severe.

To illustrate, assume that the wave-front control goal is to maximize performance metric (4) and that J_l is the lth local maximum of metric (4) achieved after compensation. With expression (4) the metric local extremum value J_l can be symbolically represented as a scalar product of two vectors: $J_l = (\boldsymbol{\beta}\mathbf{j}_l)$, where $\boldsymbol{\beta} = \{\beta_j\}$ is the vector for the weighting coefficients in Eq. (4) and $\mathbf{j}_l = \{j_{l,j}\}$ is the metric vector corresponding to the lth local extremum. The vector $\mathbf{j}_l$ is composed of the metric components $\{j_{l,j}\}$ obtained from each of the N_g wave-front sensors.

Consider the following assumption based on the numerical analysis described below. For reference waves separated by angular distances exceeding the isoplanatic angle θ_0 (anisoplanatic references), the most likely local maximum of metric (4) is associated with optimization (maximization) of a single component of the metric vector $\mathbf{j} = \{j_j\}$ and a decrease in all of the other components. In other words, the optimization process results in compensation corresponding to a single reference and disregards the phase-aberration information obtained from sensing the other reference waves. Which of the local maxima traps the adaptation process depends on the initial conditions (metric vector $\mathbf{j}^0 = \{j_j^0\}$) and on the selected weighting coefficients $\{\beta_j\}$.

The set of metric vectors $\mathbf{j}_l$ ($l = 1,..., N_g$) associated with the most likely local maxima of metric (4) can be represented in the form

$$\mathbf{j}_l = \{0,..., 0, j_l, 0,..., 0\}, \quad (5)$$

where j_l is the stationary-state metric value corresponding to the lth reference, the reference "winner." We neglect here the presence of noise in measurement of the metric-vector components. The value of metric (4) corresponding to this "winning" reference (guide-star) is $J_l = (\boldsymbol{\beta}\mathbf{j}_l) = \beta_l j_l$.

The evolution (convergence) process characterized by solutions of type (5) is known in artificial neural network theory as winner-takes-all (WTA) dynamics.[22] Thus optimization of metric (4) by the adaptive receiver system with multiple reference sources can result in phase distortion compensation only for a single reference source (winning guide star). This compensation process occurs in the form of WTA competition. The potential advantages in using multiple references instead of a single reference wave can be realized only if the WTA dynamics of the closed-loop control system are somehow destroyed.

D. Multireference Decoupled Stochastic Parallel Gradient Descent Control Algorithm

As an example of closed-loop compensation with "destroyed" interreference WTA competition, consider a closed-loop compensation system with two reference waves (A and B). The angular distance between these two waves is θ_{AB} (see Figs. 3b and 3c). Assume that adaptive compensation is based on optimization (minimization) of the near-field performance metric J_3^{AB} in Eq. (3). The advantage of metric J_3^{AB} is that it can be optimized by using both SPGD and D-SPGD controllers.

The D-SPGD iterative procedure for control signal update described in Part I for a single reference [see Eq. (2) in Ref. 1] can be generalized to include multiple-reference compensation. For two reference waves it can be represented in the form

$$u_j^{(n+1)} = u_j^{(n)} + \gamma^{(n)}[\beta_A^n \delta\bar{I}_j^{A(n)} + \beta_B^n \delta\bar{I}_j^{B(n)}]\delta u_j^{(n)}$$

$$(j = 1,..., N). \quad (6)$$

Here $\{\delta u_j^{(n)}\}$ are random control signal perturbations applied to the corrector actuators that are dependent on the iteration number n, $\{\delta\bar{I}_j^{A(n)}\}$ and $\{\delta\bar{I}_j^{B(n)}\}$ are the corresponding variations in the sensors' output signals (metric-vector components), and $\{\beta_A^n\}$ and $\{\beta_B^n\}$ are weighting coefficients.

To avoid WTA-type competition that can lead to a local extremum for the metric J_3^{AB} associated with one of the two reference waves, introduce the following iterative procedure for weighting coefficient update in Eq. (6):

$$\beta_A^{(n)} = \frac{St_B^{(n)}}{St_A^{(n)} + St_B^{(n)}}, \qquad \beta_B^{(n)} = \frac{St_A^{(n)}}{St_A^{(n)} + St_B^{(n)}}, \quad (7)$$

where $St_A^{(n)}$ and $St_B^{(n)}$ are the Strehl ratio components at the nth iteration registered by the two far-field sensors shown in Fig. 3b.

The weighting coefficient update rule (7) penalizes the advantage (success) in compensating each of the residual
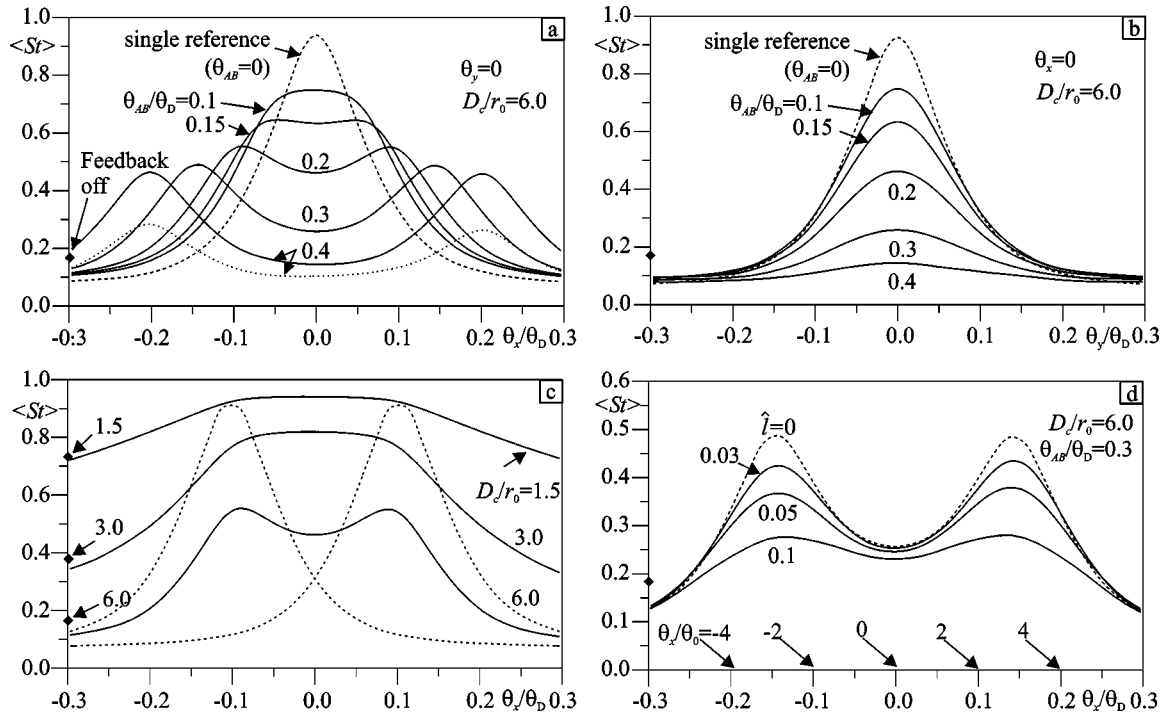
Fig. 4. Extended-FOV D-SPGD compensation with two reference waves and a single wave-front corrector.   Ensemble-averaged Strehl ratio profiles $\langle St(\theta_x, \theta_y = 0)\rangle$ in a, c, and d and $\langle St(\theta_x = 0, \theta_y)\rangle$ in b are obtained after MR D-SPGD compensation: a and b correspond to different angular distances θ_{AB} between the reference waves ($D_c/r_0 = 6.0$), and c corresponds to different parameters D_c/r_0 with $\theta_{AB}/\theta_D = 0.2$. The dashed curves in both a and b correspond to compensation with a single reference wave. The dashed curves in c correspond to a D-SPGD process converging to a local minimum for $D_c/r_0 = 6.0$. The dotted curve in a is obtained for $\theta_{AB}/\theta_D = 0.4$ with partitioning of the wave-front corrector area into two sections, each with 16×32 actuators. Each section is controlled with a separate wave-front sensor. The Strehl ratio profiles in a–c are obtained in the near-field approximation, and d corresponds to the quasi-optical approximation for different propagation distances l/l_d. The dashed curve in d corresponds to the near-field approximation. In d, the Strehl ratio profiles are shown for offset angles normalized by both the angle θ_D and the isoplanatic angle θ_0 (indicated by arrows).

wave-front phase-aberration components, thus preventing the adaptive process from converging to a single-reference solution, a local minimum of metric (3). If at the nth iteration $St_A^{(n)} > St_B^{(n)}$, from Eq. (7) it follows that $\beta_A^n < \beta_B^n$.

The D-SPGD control algorithm (6) with the weighting coefficient update rule (7) is referred to as multiple-reference D-SPGD (MR D-SPGD). The schematic for the MR D-SPGD adaptive optics receiver system is shown in Fig. 3b. The control system includes two near-field narrow-FOV wave-front sensors (sensors A and B) used for sensing the metric-vector components $\{\delta \bar{I}_j^{A(n)}\}$ and $\{\delta \bar{I}_j^{B(n)}\}$ and two far-field sensors providing measurements of the on-axis focal plane irradiance (or the corresponding Strehl ratios St_A and St_B) used for computing the weighting coefficients $\{\beta_A^n\}$ and $\{\beta_B^n\}$.

Expression (7) can be generalized to include the constellation of N_g reference sources. In this case a weighting coefficient associated with the jth reference wave is given by the following expression:

$$\beta_j^{(n)} = \sum_{l \neq j}^{N_g} St_l^{(n)} \bigg/ \sum_{l=1}^{N_g} St_l^{(n)}, \qquad (8)$$

where $\{St_l^{(n)}\}$ are the Strehl ratios measured for each of the N_g reference sources. The D-SPGD control algorithm (6) for multiple-reference operation is given by

$$u_j^{(n+1)} = u_j^{(n)} + \gamma^{(n)} \sum_{l=1}^{N_g} \beta_l^n \, \delta \bar{I}_{j,l}^{(n)} \, \delta u_j^{(n)} \qquad (j = 1,..., N),$$

$$(9)$$

where $\delta \bar{I}_{j,l}^{(n)}$ is the jth component of the lth sensor's output signal variation.

4. EXTENDED-FIELD-OF-VIEW COMPENSATION WITH MULTIPLE REFERENCES

A. Extended-Field-of-View Compensation with Two References

Consider an extended-FOV compensation system with two reference sources and a single wave-front corrector (32×32 element piston-type corrector array) in the receiver system pupil plane, as shown in Fig. 3b. Phase-distortion compensation is performed by using the MR D-SPGD controller (6) with the weighting coefficient update rule (7).

Results of adaptive compensation are presented in Figs. 4a and 4b for two reference waves separated by various angular distances θ_{AB}/θ_D ($\theta_D = D_c/l$). The adaptive optics system FOV is estimated by using the angular dependence of the ensemble-averaged Strehl ratio $\langle St(\boldsymbol{\theta})\rangle$, where $\boldsymbol{\theta} = \{\theta_x, \theta_y\}$ is the angular vector with angular coordinates θ_x and θ_y. The angular vector $\boldsymbol{\theta}$ is associated

with the wavevector $\mathbf{k}_\theta = k\{\cos\theta_x, \cos\theta_y\} (k = 2\pi/\lambda)$. The angular vectors of the reference waves $\boldsymbol{\theta}_A = \{-\theta_{AB}/2, 0\}$ and $\boldsymbol{\theta}_B = \{\theta_{AB}/2, 0\}$ correspond to the wave vectors $\mathbf{k}_A$ and $\mathbf{k}_B$ shown in Fig. 3c.

Figures 4a and 4b represent two orthogonal profiles of the averaged Strehl ratio function: $\langle St(\theta_x, \theta_y = 0)\rangle$ in Fig. 4a and $\langle St(\theta_x = 0, \theta_y)\rangle$ in Fig. 4b. The Strehl ratio function $\langle St(\theta_x, 0)\rangle$ in Fig. 4a is shown for fixed turbulence strength ($D_c/r_0 = 6.0$) and different values of the normalized angular distance θ_{AB}/θ_D between the two reference waves. As seen from a comparison of the single (dashed curve in Fig. 4a) with the two-reference compensation, the use of two reference waves increases the receiver system FOV beyond the range that can be achieved with the use of a single reference. As seen in Fig. 4b, the increase in the receiver system FOV in one direction (θ_x direction) has little effect on the receiver system FOV in the orthogonal θ_y direction.

As θ_{AB} increases, the FOV increase in the θ_x direction is accompanied by a certain decrease in compensation performance in the central (on-axis) angular region. For $\theta_{AB} > 0.2\theta_D$, the Strehl ratio curves in Fig. 4a have two noticeable maxima at the angular distances $\theta_x = -\theta_{AB}/2$ and $\theta_x = \theta_{AB}/2$ that correspond to the angular directions of the two reference sources, with a minimum at $\theta_x = 0$.

This result is easy to understand. For a relatively large angular distance θ_{AB} between the reference waves, the associated phase-distortion components, $\varphi_A(\mathbf{r})$ and $\varphi_B(\mathbf{r})$, and the corresponding wave-front sensor outputs are practically uncorrelated. Optimizing metric (3) results in a complicated partitioning of the wave-front corrector area between the regions associated with aberration compensation for each of the two reference waves. Note that such wave-front corrector area partitioning occurs only with the use of the MR D-SPGD control algorithm, which penalizes the most successfully operating subsystem at each iteration of the control signal update. Adaptive correction performed with the constant weighting coefficients in Eq. (6), the conventional D-SPGD controller, collapses to one of the two local minima of metric (3) that corresponds to single-reference compensation. Examples of conventional D-SPGD controller convergence to local minima are shown in Fig. 4c for $D_c/r_0 = 6$ (dashed curves).

Compare the compensation efficiency in Fig. 4a for the angular distance $\theta_{AB} = 0.4\theta_D$ obtained by using the MR D-SPGD controller (solid curve) with what can be achieved by two independent adaptive optics subsystems that use two different single reference sources but share the same wave-front corrector by equally dividing its area between the two subsystems (two corrector areas with 16×32 elements each). Each of these adaptive optics subsystems compensates phase aberrations that correspond to only one of the two reference waves. The Strehl ratio values for this system (shown by the dotted curve in Fig. 4a) are smaller than the Strehl ratio values obtained with the MR D-SPGD controller. Thus the MR D-SPGD control algorithm provides more efficient sharing of the wave-front corrector resources between the two compensation directions than can be obtained with a direct split of wave-front corrector area.

Consider the Strehl ratio profiles $\langle St(\theta_x, 0)\rangle$ in Fig. 4c

obtained for a fixed angular distance $\theta_{AB} = 0.2\theta_D$ between the two reference waves, and for different D_c/r_0 ratio values. For relatively weak turbulence ($D_c/r_0 \leqslant 3$), the pupil-plane phase aberrations $\varphi_A(\mathbf{r})$ and $\varphi_B(\mathbf{r})$ are strongly correlated. This results in the appearance of a flat top in the Strehl ratio curve $\langle St(\theta_x, 0)\rangle$ in Fig. 4c. In this angular region the compensated receiver system FOV is nearly uniform in the θ_x direction.

As the ratio of D_c/r_0 increases, the correlation between the phase aberrations $\varphi_A(\mathbf{r})$ and $\varphi_B(\mathbf{r})$ decreases. This results in the appearance of two well-resolved maxima in the Strehl ratio curve $\langle St(\theta_x, 0)\rangle$ at the off-axis angles $\theta_x = \theta_{AB}/2$ and $\theta_x = -\theta_{AB}/2$, as shown in Fig. 4c for $D_c/r_0 = 6$.

The ensemble-averaged Strehl ratio curves in Figs. 4a–4c were obtained with the phase-aberration projection (near-field) approximation [$\varphi_p(\mathbf{r}) = \varphi(\mathbf{r})$], which does not take into account diffraction effects. In Fig. 4d the angular dependence of the compensated Strehl ratio $\langle St(\theta_x, 0)\rangle$ for the near-field approximation (dashed curve) is compared with the corresponding dependencies (solid curves) obtained by considering wave diffraction along the propagation path between the distorting layer and the receiver telescope pupil plane (quasi-optical approximation). As the propagation distance l increases, overall compensation efficiency declines while the angular dependence $\langle St(\theta_x, 0)\rangle$ becomes more uniform.

B. Two-Reference Decoupled Stochastic Parallel Gradient Descent Compensation and Wave-Front Corrector Resolution

Compare the efficiency of MR D-SPGD compensation with two reference waves for wave-front correctors having a different number of actuators $N = n_c \times n_c$. The compensated Strehl ratio profiles $\langle St(\theta_x, 0)\rangle$ and $\langle St(0, \theta_y)\rangle$ for different N and a fixed angular distance $\theta_{AB} = 0.2\theta_D$ between the two reference waves are shown in Fig. 5 (near-field approximation).

As seen from Fig. 5a, increasing the wave-front corrector actuator number above $N = 8 \times 8$ results in an improvement of compensation efficiency primarily in the angular regions located near the reference wave propagation directions $\theta = \pm\theta_{AB}/2$. However, the increase in the Strehl ratio near the reference wave directions is accompanied by a decline in on-axis compensation efficiency (compare the Strehl ratio profiles in Fig. 5a for $N = 8 \times 8$ with $N \geqslant 16 \times 16$). This result is not unexpected. Performance metric (3) optimized by the MR D-SPGD controller depends solely on the narrow FOV wave-front sensor output intensities obtained only for the reference waves. This metric does not penalize residual phase aberrations in the on-axis direction. As seen from the Strehl ratio curves in Fig. 5a, increasing the wave-front corrector spatial resolution does not necessarily result in improvement in adaptive optics system performance (spatially uniform extension of the receiver system FOV) when two angularly separated reference waves are used for compensation.

Thus, to avoid the appearance of bumps in the Strehl ratio profile (while still extending the receiver system FOV), the wave-front corrector should have enough actuators for compensation of the phase aberration components

that are spatially correlated for both reference waves. The additional actuators are not utilized by the MR D-SPGD control system to uniformly increase the Strehl ratio but rather to improve compensation performance in the angular vicinities of the reference sources by compensating weakly correlated small-scale phase-aberration components present in the phase aberration of each reference wave. The spatial resolution of the wave-front corrector (number of actuators N) resulting in the most flat Strehl ratio curve $\langle St(0, \theta_y)\rangle$ in Fig. 5a corresponds to $N = 8 \times 8$. As seen in Fig. 5b, the same number of wave-front corrector actuators $N = 8 \times 8$ also provides the best compensation performance [the largest Strehl ratio $\langle St(0, \theta_y)\rangle$] in the orthogonal angular direction. Note that the optimal wave-front corrector spatial resolution depends on both the angular distance θ_{AB} between the reference sources and the turbulence strength (D_c/r_0 ratio).

C. Anisotropic-Field-of-View Widening

As seen from Figs. 4 and 5, the use of two reference sources results in a highly nonuniform (anisotropic) FOV in the two orthogonal viewing directions. Spatial aniso-
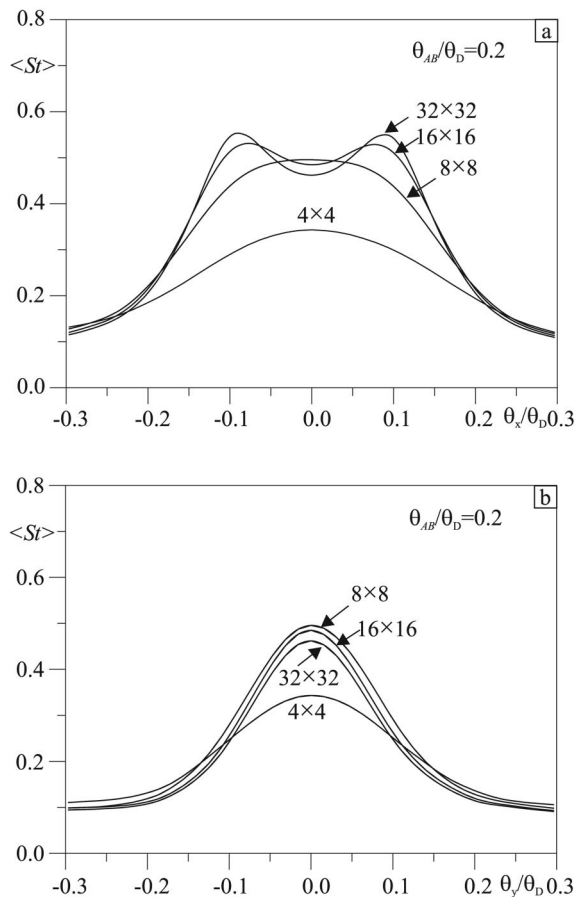

Fig. 5. Effect of wave-front corrector resolution on phase-aberration compensation efficiency with two reference waves for the near-field approximation and $D_c/r_0 = 6$. The ensemble-averaged Strehl ratio profiles $\langle St(\theta_x, 0)\rangle$, a and $\langle St(0, \theta_y)\rangle$, b, correspond to a piston-type wave-front corrector array with different numbers of actuators N. Control parameters are optimized separately for each N in a and b.

tropy of the receiver system FOV in selected angular directions may be required for such adaptive optics applications as illumination and tracking and imaging of objects that are extended in one direction (cigar-shaped objects). For a bright (or laser-illuminated) object, reference waves with the required angular separation can be selected directly from the received light by using two narrow-FOV wave-front sensors with an angularly shifted optical axis.

The major advantage of anisotropic compensation (for one direction only) with two references is the improved utilization of the compensation resources (wave-front corrector area). In this case the corrector active area (actuators) is not wasted so as to improve the system FOV in nonessential directions. Note that two-reference D-SPGD adaptive optics compensation does not require knowledge of the location and strength of the distorting layers, the major drawback for most multiconjugate compensation approaches.[11,23,24] On the other hand, although MR D-SPGD adaptive optics compensation with a single corrector does increase the system FOV, it still cannot provide diffraction-limited compensation.

The performance of the MR D-SPGD adaptive optics system with a single corrector and two wave-front sensors is strongly dependent on the spatial correlation between wave-front aberrations of the selected references. The aim of the control algorithm is to find and compensate these highly correlated phase-aberration components to achieve a simultaneous "compromised" improvement for both reference directions. This type of compromise leads to some decrease in compensation performance in comparison with a single reference case. For the case in which the correlation between phase aberrations of the reference waves is weak, the MR D-SPGD adaptive optics system operates as two quasi-independent single-reference systems. This leads to a complicated wave-front corrector partitioning that provides nearly equal compensation performance for both reference directions.

D. Extended-Field-of-View Compensation for Three Reference Waves

For the case of extended targets (in two dimensions) as well as for most imaging applications (e.g., astronomical imaging), the use of two reference sources is not sufficient and cannot provide a spatially uniform increase in the receiver system FOV. Adaptive optics compensation may require the use of several (at least more than two) reference sources.

Consider an example of the MR D-SPGD adaptive receiver system operating with three reference waves that propagate through a single distant phase-distorting layer. In the angular space of the propagation directions, the group of the three reference waves (A, B, C) represents an equilateral triangle with an angular distance between the references of $\theta_{AB} = \theta_{BC} = \theta_{CA} = \theta_s$. The telescope optical axis is orthogonal to this triangle and passes through its middle point, as shown in Fig. 6. In this case, the angular coordinates for the reference wave propagation directions are $\boldsymbol{\theta}_A = (-\theta_s/2, -\sqrt{3}\,\theta_s/4)$, $\boldsymbol{\theta}_B = (\theta_s/2, -\sqrt{3}\,\theta_s/4)$, and $\boldsymbol{\theta}_C = (0, \sqrt{3}\,\theta_s/4)$.

Compensation efficiency of the three-reference MR D-SPGD adaptive optics system is analyzed by using the
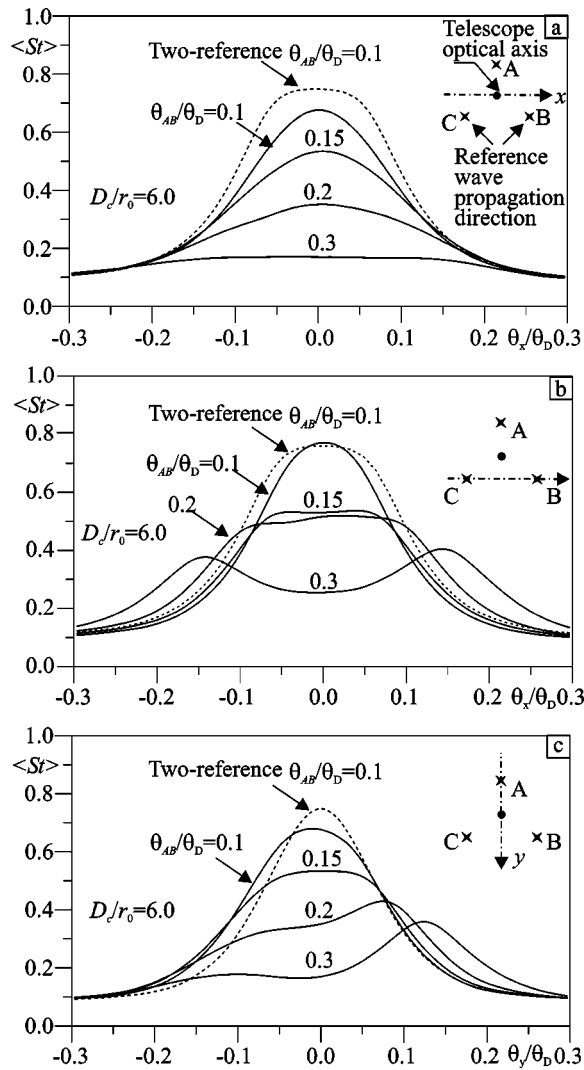
Fig. 6. Extended-FOV D-SPGD compensation with three reference waves and a single wave-front corrector, for ensemble-averaged Strehl ratio profiles $\langle St(\theta_x, 0)\rangle$, a; $\langle St(\theta_x, -\sqrt{3}\,\theta_s/4)\rangle$, b; and $\langle St(0, \theta_y)\rangle$, c. The dashed curves in a–c correspond to results obtained for two-reference compensation with an angular distance $\theta_{AB}/\theta_D = 0.1$. The geometry indicating reference wave propagation directions is illustrated in the right top corner of a–c.

near-field approximation. The obtained ensemble-averaged Strehl ratio profiles $\langle St(\theta_x, 0)\rangle$ and $\langle St(0, \theta_y)\rangle$ for different angular distances θ_s are shown in Figs. 6a and 6c.

In comparison with two-reference compensation (dashed curves), the Strehl ratio profiles $\langle St(\theta_x, 0)\rangle$ for the three-reference wave configuration in Fig. 6a is narrower. As the angular distance θ_s between the references increases, the compensated Strehl ratio values $\langle St(\theta_x, 0)\rangle$ became smaller over the entire compensation angular range (compare with the Strehl ratio curves in Fig. 6a).

The Strehl ratio profile along the angular direction $\theta = (\theta_x, -\sqrt{3}\,\theta_s/4)$, which includes the angular coordinates of the two reference sources (B and C), is shown in Fig. 6b. Similarly to the two-reference configuration, the Strehl ratio profile exhibits two local maxima that coin-

cide with the angular vectors θ_B and θ_C of the two reference waves, although the achieved Strehl ratio value is less than for the two-reference compensation in Fig. 4a.

Examine compensation efficiency in the orthogonal (θ_y) direction that includes the angular coordinate θ_B of the reference source B (Fig. 6c). The adaptive receiver FOV in this case is slightly wider than for the two-reference system, as can be seen by comparing the Strehl ratio profiles $\langle St(0, \theta_y)\rangle$ for three-reference (solid curves) compensation with the profile for two-reference (dashed curve) compensation.

Although three-reference compensation provides a more spatially uniform FOV than does two-reference compensation, the increase in the number of reference waves is accompanied by a general decrease in the achieved Strehl ratio values.

5. CONCLUSIONS

In this paper we analyzed adaptive compensation of wave-front phase aberrations in optical receiver systems when the propagation medium's refractive-index inhomogeneties are distributed along the propagation path and cannot be accurately modeled by a single pupil-plane phase-distorting layer. The model used for the propagation medium's refractive-index fluctuations included a single or a set of remotely located thin phase screens (distance phase screens). Wave propagation through a layered phase-distorting medium may result in strong intensity scintillations at the receiver aperture as well as the appearance of topological singularities of the pupil-plane phase (phase branch points). Both effects strongly affect wave-front control techniques and are the principle problems with conventional adaptive optics techniques based on wave-front phase reconstruction and phase conjugation.

The distant location of the phase-distorting layers introduces an additional problem related to anisoplanatic effects when phase aberrations at the receiver pupil plane depend on the wave-front angle of arrival. The efficiency of adaptive correction performed for an optical wave propagating along the optical axis degrades when the wave-front angle of arrival increases, thus imposing a limitation on the receiver system field of view (FOV).

We analyzed adaptive system architectures based on the decoupled stochastic parallel gradient descent (D-SPGD) algorithm applied to an adaptive optics system with piston-type wave-front corrector (two-dimensional array of piston actuators) and point-diffraction interferometer-type wave-front sensor. As shown in Part I (see Ref. 1), for narrow FOV receiver systems, D-SPGD feedback control provides robust and efficient operation even in conditions of strong intensity scintillations. Here in Part II we analyzed the compensated receiver system FOV and the possibility of controlling the system FOV (extended FOV compensation) by using AO system architectures with several wave-front sensors that provide sensing of wave-front phase aberrations for different arrival angles.

The conventional D-SPGD control algorithm can be modified to include (fuse) output signals from multiple wave-front sensors. As shown in the analysis, the main problem with the conventional D-SPGD control approach

is the existence of local control system states in which feedback control is based solely on the output signal from a single sensor (wave-front sensor "winner") and all other sensor outputs are ignored—a winner-takes-all (WTA) type of dynamics of the closed-loop operation.

To prevent WTA competition between phase-distortion information obtained from different wave-front sensors, we introduced the multiple-reference D-SPGD (MR D-SPGD) algorithm. This algorithm was applied to form an anisotropic FOV in the adaptive optics receiver system—a FOV extended in one angular direction. The control system is composed of a MR D-SPGD feedback controller operating with two wave-front sensors and a single wave-front corrector. The adaptive optics receiver system with anisotropic FOV can be applied for imaging and tracking of cigar-shaped objects without the need for multiconjugate adaptive optics compensation with multiple correctors and wave-front sensors.

The MR D-SPGD control technique can also be applied, to some extent, to dynamically form the adaptive optics system FOV by rearranging multiple guide stars used for adaptation or by tracking the moving reference light sources (satellites, space debris, etc.).

ACKNOWLEDGMENTS

REFERENCES

1. M. Yu and M. A. Vorontsov, "Compensation of distant phase-distorting layers. I. Narrow-field-of-view adaptive receiver," J. Opt. Soc. Am. A **21**, 1645–1658 (2004).
2. M. A. Vorontsov and V. P. Sivokon, "Stochastic parallel-gradient-descent technique for high-resolution wave-front phase-distortion correction," J. Opt. Soc. Am. A **15**, 2745–2758 (1998).
3. M. A. Vorontsov, G. W. Garhart, M. Cohen, and G. Cauwenberghs, "Adaptive optics based on analog parallel stochastic optimization: analysis and experimental demonstration," J. Opt. Soc. Am. A **17**, 1440–1453 (2000).
4. M. A. Vorontsov, "Decoupled stochastic parallel gradient descent optimization for adaptive optics: integrated approach for wave-front sensor information fusion," J. Opt. Soc. Am. A **19**, 356–368 (2002).
5. J. W. Hardy, *Adaptive Optics for Astronomical Telescopes* (Oxford U. Press, New York, 1998).
6. D. L. Fried, "Anisoplanatism in adaptive optics," J. Opt. Soc. Am. **72**, 52–56 (1982).
7. F. Roddier, *Adaptive Optics in Astronomy* (Cambridge U. Press, New York, 1999).
8. T. Fusco, J. M. Conan, L. M. Mugnier, V. Michau, and G. Rousset, "Characterization of adaptive optics point spread function for anisoplanatic imaging: application to stellar field deconvolution," Astron. Astrophys. **142**, 149–156 (2000).
9. B. L. Ellerbroek, "First-order performance evaluation of adaptive-optics systems for atmospheric-turbulence compensation in extended-field-of-view astronomical telescopes," J. Opt. Soc. Am. A **11**, 783–805 (1994).
10. B. L. Ellerbroek and F. Rigaut, "Methods for correcting tilt anisoplanatism in laser-guide-star-based multiconjugate adaptive optics," J. Opt. Soc. Am. A **18**, 2539–2547 (2001).
11. D. C. Johnson and B. M. Welsh, "Analysis of multiconjugate adaptive optics," J. Opt. Soc. Am. A **11**, 394–408 (1994).
12. V. V. Voitsekhovich and S. Bara, "Effect of anisotropic imaging in off-axis adaptive astronomical systems," Astron. Astrophys., Suppl. Ser. **137**, 385–389 (1999).
13. N. Ageorges and C. Dainty, *Laser Guide Star Adaptive Optics for Astronomy* (Kluwer Academic, Dordrecht, The Netherlands, 2000).
14. J. L. Beuzit, N. Hubin, E. Gendron, L. Demailly, P. Gigan, F. Lacombe, F. Chazallet, D. Rabaud, and G. Rousset, "Adonis: a user-friendly adaptive optics system for the ESO 3.6 meter telescope," in *Adaptive Optics in Astronomy*, F. Merkle, ed., Proc. SPIE **2201**, 955–960 (1994).
15. E. Kibblewhite, "Laser beacons for astronomy," in *Laser Guide Star Adaptive Optics*, R. Q. Fugate, ed. (Philips Laboratory, Kirtland Air Force Base, N.M., 1992), pp. 24–36.
16. M. Tallon and R. Foy, "Adaptive telescope with laser probe: isoplanatism and cone effect," Astron. Astrophys. **235**, 549–557 (1990).
17. B. M. Welsh and C. S. Gardner, "Effects of turbulence-induced anisoplanatism on the imaging performance of adaptive-astronomical telescopes using laser guide stars," J. Opt. Soc. Am. A **8**, 69–80 (1991).
18. M. Le Louarn, "Multi-conjugated adaptive optics with laser guide stars: performance in the infrared and visible," Mon. Not. R. Astron. Soc. **334**, 865–874 (2002).
19. M. Le Louarn and M. Tallon, "Analysis of modes and behavior of a multiconjugate adaptive optics system," J. Opt. Soc. Am. A **19**, 912–925 (2002).
20. T. R. O'Meara, "The multi-dither principle in adaptive optics," J. Opt. Soc. Am. **67**, 306–315 (1977).
21. J. C. Spall, *Introduction to Stochastic Search and Optimization* (Wiley, New York, 2003).
22. A. Cichocki and R. Unbehauen, *Neural Networks for Optimization and Signal Processing* (Wiley, New York, 1993).
23. C. Flicker, "Sequence of phase correction in multiconjugate adaptive optics," Opt. Lett. **26**, 1743–1745 (2001).
24. A. Tokovinin, M. Le Louarn, and M. Sarazin, "Isoplanatism in multi-conjugate adaptive optics systems," J. Opt. Soc. Am. A **17**, 1819–1827 (2000).